Reports

Estimate of Electromagnetic Quantities in Space from Ground Magnetic Records

Y. KAMIDE

Magnetic field records at the earth's surface contain the effects of a variety of different source currents flowing in outer space. During the last decade, several computational techniques for the use of magnetometer data have been proposed to obtain the global pattern of the electric fields and currents and Joule heating in the ionosphere. The numerical algorithm has now been enormously improved, such that simultaneous more direct or in situ measurements by satellites and radars can be incorporated into the scheme. In particular, owing to recent progress in satellite-viewed auroral images, it is possible to estimate "instantaneous" patterns of the ionospheric electrodynamic quantities over the entire polar region with a time resolution of several minutes. This report demonstrates that, contrary to our conventional views, large ionospheric currents can flow in regions of low auroral activity.

GEOMAGNETIC FIELD VECTORS ARE routinely measured at some 200 observatories on the ground, providing useful information on what is happening in space around the earth. The so-called magnetogram-inversion methods enable us to sense the electrodynamic state of our earth's environment, including the ionosphere and the magnetosphere, as well as their coupling (*1*). Figure 1 shows a block diagram, outlining the physical processes occurring in the earth's magnetosphere-ionosphere system. One of the points emphasized by this diagram is that ground magnetic perturbations recorded at high latitudes are, under certain approximations (*2*), the direct effects of two dominant currents, the ionospheric "horizontal" current and the "vertical" current flowing along magnetic field lines. Kisabeth (*3*) has attempted to separate quantitatively the ground magnetic effects from these two currents. Others (*2, 4*) have developed more advanced techniques in which not only currents but also electric fields can be determined primarily from ground-based magnetic records. In fact, many recent studies, combined with the rapid progress in the systematic data-gathering program during the 1976–1979 IMS (International Magnetospheric Study) period, have proven that these "remote sensing" schemes are quite powerful in estimating electromagnetic quantities on a global scale (*5*).

It must be noted, however, that, unlike rocket and satellite measurements, the derivation of ionospheric parameters by means of the magnetogram-inversion scheme is not based on in situ data, but on indirect measurements. Further, although a realistic model of the dyadic ionospheric conductivities must be given, there is at present no simple way the conductance over the entire polar region can be properly measured on an instantaneous basis (*6*). In view of the somewhat high degree to which the electric field and Joule heat production rate depend on the assumption of the ionospheric conductivity distribution (*7*), crucial comparisons must be conducted between the results estimated from magnetogram-inversion techniques and those observed by more direct methods. This is why the application of the inversion methods has been limited mostly to statistical data sets of magnetic variations or to empirical conductivity models (*8*).

The recent availability of radar and satellite data at high latitudes tends to provide us with a unique opportunity to make an optimized estimate of the electrodynamic features (*9*). It is useful to improve the numerical schemes in such a way that simultaneous, "more direct" measurements of electric fields, conductivities, and field-aligned currents can be incorporated into the magnetogram-inversion algorithms.

The algorithm discussed in this report has now been improved in the following three ways: First, the auroral enhancement component of the ionospheric conductance has been calculated on the basis of global images of auroral emissions observed from 20,000-km altitude with Dynamics Explorer (DE) 1 (*10*), instead of employing the statistical models (*11*) that were used extensively in earlier studies. Although the absolute values of the estimated conductivity need further cross-calibrations with elaborate calculations relating to the excitation of ionospheric constituents caused by precipitating electrons (*12*), the region of aurorally enhanced conductivities is fairly accurately determined, making it possible to infer the distribution of the three-dimensional current system (*13*). In the second form of improvement, many different types of simultaneous measurements can be used, such as electric fields and ionospheric conductivities from

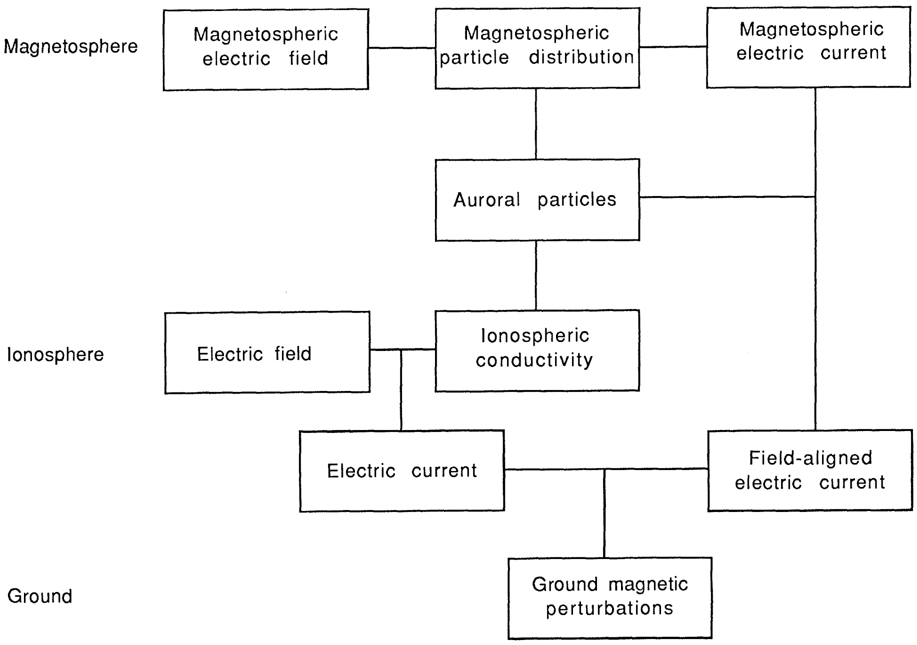

Fig. 1. Schematic diagram showing electrodynamic coupling between the earth's magnetosphere and the ionosphere.

Faculty of Science, Kyoto Sangyo University, Kita-ku, Kyoto 603, Japan.

radars and polar-orbiting satellites, field-aligned currents from satellites and ionospheric currents from radars, as well as ground-based magnetic perturbations (*14*). One of the advantages of the new algorithm is that it can quantify the errors inherent in mapping the electric fields, thus demanding more specific quantitative input. Third, a realistic instantaneous conductivity distribution deduced from bremsstrahlung x-ray image data from a polar-orbiting spacecraft has been combined with the magnetogram-inversion technique (*15*). The satellite x-ray imagery has a great advantage in that the scanning detector can image a large portion of the auroral belt under both sunlit and non-sunlit conditions.

Through this series of improvements, a number of important characteristics, which were not explicit in earlier studies, have become evident, even though the global patterns in individual cases are quite variable depending upon solar wind conditions and geomagnetic activity. One of the characteristics seen repeatedly in the deduced diagrams of the global electrodynamic features is that a significant amount of ionospheric currents can flow in regions where auroral activity and the corresponding conductivity are quite low. That is, the region of the intense auroral electrojets is not completely the same as the region of the high conductivity and that of the large electric field, there being latitudinal shifts among these three quantities. This effect is particularly significant over the poleward half of the westward electrojet in the morning sector, where the electric field combined with relatively low conductance is the main contributor to the ionospheric current. On the other hand, the equatorward half of the auroral electrojet is dominated by conductivity enhancements, signaling high auroral activity. Such a finding is hardly expected from studies in which statistically derived models of the ionospheric conductivity and of the electric field are independently given.

Figure 2A shows latitudinal profiles of the three quantities (the electric field, the conductance, and their product, the current) overlaid for 0400 MLT (magnetic local time). These quantities have been deduced from the best optimized result using nearly simultaneous data of DE 1 auroral imagery and of DE 2 ion drift, in addition to ground magnetometer records for the maximum epoch of an intense disturbance. It is clear that the electric field peaks poleward of 69° latitude, whereas the highest conductivity occurs somewhat southward of it, extending to 64° latitude in this particular example, implying that enhancements in the electric field and in auroral activity control the strength of the electrojet current separately. The peak of the westward electrojet is located between the two peaks (*16*).

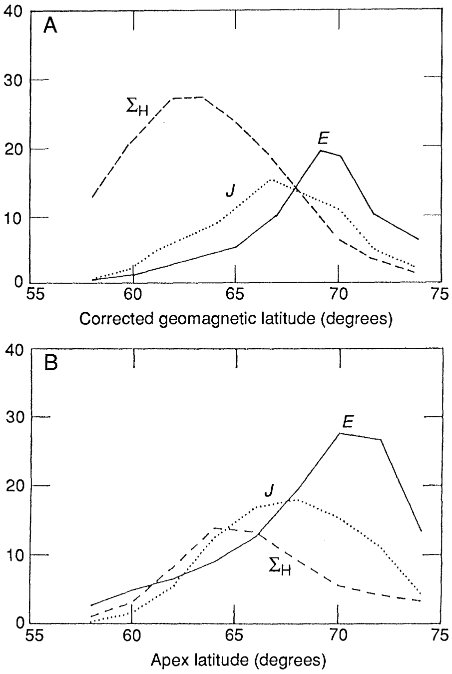

Fig. 2. (**A**) Individual latitudinal distribution of the electric field *E*, the Hall conductivity Σ_H, and the Hall current *J* for 0400 MLT, calculated through the magnetogram-inversion technique for 1252 UT, 12 December 1981. Vertical scale units: *E*, millivolts per meter; Σ_H, mhos; *J*, 0.1 A/m. (**B**) Statistical profile of the three quantities, after Foster (1987). Foster *et al.* (*18*) obtained the distribution of ionospheric convection determined from Millstone Hill radar data for different intensities of auroral particle precipitation, using a precipitation index based on spacecraft observations (*6*). This diagram is for index level 7.

Figure 2B is a sample of the latitudinal profiles of the three parameters (*17*) for 0400 MLT for active times, which are based on a statistical study of the convection electric fields from the Millstone Hill radar and of particle precipitation from the NOAA/TIROS satellites (*18*). Although the exact locations of the three quantities and their magnitudes are different between the individual case shown in Fig. 2A and the average case, the latitudinal separation of the electric field and conductivity peaks by several degrees is consistently noticed. This offset is important because it has been a common practice to assume tacitly that the auroral electrojets, as the terminology implies, are flowing in the region of high conductance where the auroral luminosity is highest.

It is noted that an earlier statistical study of the auroral electrojets at different local times has indicated that the auroral electrojets may have two different elements: the electric field–dominant electrojet and the conductivity-dominant electrojet (*19*). Combining the statistical indication and the present finding, it is inferred that the auroral electrojets do not grow and decay as a whole, but only the portion in the midnight sector and the equatorward half of the currents is enhanced at the time of auroral breakup and the other portion is controlled by the electric field, which does not primarily reflect auroral activity. Further, the implications of these two elements are interesting if they are viewed as two physical processes for solar wind–magnetosphere energy coupling, that is, the directly driven and loading-unloading processes (*20*). The "electric field" electrojet may represent directly the effects of the solar wind–magnetosphere dynamo, whereas the "conductivity-rich" electrojet may be a manifestation of a plasma instability process internal to the magnetosphere, relating to intense and sporadic auroral activity.

REFERENCES AND NOTES

1. K.-H. Glaßmeier, *Ann. Geophys.* **5A**, 115 (1987).
2. Y. Kamide, A. D. Richmond, S. Matsushita, *J. Geophys. Res.* **86**, 801 (1981).
3. J. L. Kisabeth, in *Quantitative Modeling of Magnetospheric Processes*, W. P. Olson, Ed. (American Geophysical Union, Washington, DC, 1979), pp. 473–498.
4. V. M. Mishin *et al.*, in *Dynamics of the Magnetosphere*, S.-I. Akasofu, Ed. (Reidel, Dordrecht, 1980), pp. 249–268.
5. S.-I. Akasofu and Y. Kamide, *Eos* **66**, 465 (1985).
6. T. J. Fuller-Rowell and D. S. Evans, *J. Geophys. Res.* **92**, 7606 (1987); R. M. Robinson *et al.*, *ibid.*, p. 2565.
7. Y. Kamide and A. D. Richmond, *ibid.* **87**, 8331 (1982).
8. Y. Kamide, *Space Sci. Rev.* **31**, 127 (1981); Y. Kamide *et al.*, *J. Geophys. Res.* **87**, 8228 (1982).
9. A. D. Richmond and Y. Kamide, *J. Geophys. Res.* **93**, in press.
10. L. A. Frank, J. D. Craven, J. L. Burch, J. D. Winningham, *Geophys. Res. Lett.* **9**, 1001 (1982).
11. R. W. Spiro, P. H. Reiff, L. J. Maher, Jr., *J. Geophys. Res.* **87**, 8215 (1982).
12. M. H. Rees, in *Solar-Terrestrial Physics*, R. L. Carovillano and J. M. Forbes, Ed. (Reidel, Dordrecht, 1983), pp. 753–780.
13. Assuming that the auroral emission intensity I is proportional to auroral electron-impact ionization density n_e squared (that is, $I \propto n_e^2$) and that the height-integrated conductivity Σ can be expressed as $\Sigma \propto I^{1/2}$, the conductivities over the entire polar region can be estimated from the auroral image data; see Y. Kamide *et al.* [*J. Geophys. Res.* **91**, 11235, (1986)] for details. Further, the use of simultaneous data of ion drifts from the sister satellite, DE 2, at lower altitudes (300 km) provides a unique opportunity to check the accuracy of our estimation by comparing the calculated electric fields with ion drift measurements, although such a comparison can be properly made only along DE 2 orbits. The optimum conductivity distribution can then be chosen on an iterative basis so that the resultant electric fields become consistent with DE 2 ion drifts.
14. This updated technique also makes use of available statistical information about the electrostatic potential (*18*), in such a way that in regions where any data are lacking the deduced pattern tends toward the statistical pattern.
15. B.-H. Ahn *et al.*, in preparation; in our upgrading of the numerical algorithm, we use the ionospheric conductance calculated from the precipitating electron spectrum on the basis of the x-ray image data following the so-called maximum-entropy method [D. J. Gorney *et al.*, *Report No. SSL-86 (6940-06)-06* (Aerospace Corp., Los Angeles, 1985)].

16. W. Baumjohann *et al.*, *J. Geophys. Res.* **85**, 1963 (1980).
17. J. C. Foster, *Geophys. Res. Lett.* **14**, 160 (1987).
18. J. C. Foster *et al.*, *ibid.* **13**, 656 (1986).
19. Y. Kamide and J. F. Vickrey, *J. Geophys. Res.* **88**, 7989 (1983).
20. S.-I. Akasofu, *Space Sci. Rev.* **28**, 121 (1981).
21. The author thanks W. Baumjohann and J. C. Foster for their useful comments on an early version of the manuscript. A special note of thanks is extended to B.-H. Ahn, S.-I. Akasofu, J. D. Craven, D. J. Gorney, H. W. Kroehl, Y. Ishihara, and A. D. Richmond for their collaboration. The work reported in this paper was supported in part by a grant-in-aid from the Ministry of Education, Science, and Culture in Japan.

29 March 1988; accepted 19 May 1988

Diffusion of Small Solutes in Polymer-Containing Solutions

KIT L. YAM, DONALD K. ANDERSON, ROBERT E. BUXBAUM*

Diffusion processes involving polymers are common in scientific and engineering separations and are a major component of biological functions. Analyses of these systems are usually based on versions of the Stokes-Einstein equation, although order of magnitude deviations have been observed. Presented here is a theoretical correction to the Stokes-Einstein equation containing a "local viscosity" function that combines diffusional hydrodynamics with Maxwell's treatment of electrical resistance in inhomogeneous regions. The resulting equation accurately predicts experimental diffusion data within tight bounds for polymer concentrations from 0 to 9 percent. It requires knowledge only of thermodynamics and of pure solvent and solution viscosities.

FOR THREE-COMPONENT DIFFUSION where one component is a dilute polymer, Stokes-Einstein type equations (for example, Eqs. 1 and 2) produce errors as large as 10,000 times (*1–8*). Notwithstanding, Eq. 1 is used as the basis for most correlations of protein sedimentation (*6*), polymerization (*4*), gel chromatography (*5*), and systems of biological interest (*8*), despite the presence of dilute polymers.

Several sound theoretical approaches can be used to derive Stokes-Einstein type equations (*9–13*); however, all of them contain a difficult assumption, that the mechanisms of molecular drag are identical with those of global viscosity. Thus, for ideal solutions at infinite dilution, the binary-liquid diffusion coefficient, D_{AB}, is predicted to be inversely proportional to viscosity (*1–13*):

$$D_{AB} = \frac{kT}{6\pi\eta r_A} \qquad (1)$$

where η is the solution (global) viscosity, k is the Boltzmann constant, T is temperature, and r_A is the hydrodynamic radius of the dilute diffusing species. From nonequilibrium thermodynamics (*14*), Eq. 1 becomes, for nonideal solutions,

$$D_{AB} = \frac{kT}{6\pi\eta r}\left(1 + \frac{d\ln\gamma_A}{d\ln x_A}\right) \qquad (2)$$

where γ_A and x_A are, respectively, the activity coefficient and mole fraction of species A, and r is the hydrodynamic radius of the diffusing species. Various statistical and hydrodynamic treatments have related r to molar volume; we have found those of Hartley and Crank (*15*), Protopapas *et al.* (*16*), and Perrin (*17*) particularly noteworthy (*18–20*); the fit is excellent in many systems. For engineering purposes, the effect of solvent association on r is typically dealt with by the correlation of Wilke and Chang (*21*) or through cluster diffusion correlations (*22, 23*).

Empirical corrections of Eq. 1 suggest that diffusivity is inversely proportional to a variable power of solvent viscosity (*1–6*), proportional to viscosity raised to the power of a function of molar volume (*24, 25*), or proportional to a variable power of the solvent molecular weight (*21*). Although these corrections allow successful matching of experimental data (*2–4, 21*), the fundamental justification is unclear. From statistical mechanics also come several attractive modifications generally having the form (*26, 27*)

$$D = D_0\exp(-\alpha c^{\nu}) \qquad (3)$$

where D_0 is the diffusivity in the absence of polymer, c is polymer concentration, and α and ν are constants. With appropriate constants for α and ν, Eq. 3 can be made to fit a given set of data excellently; however, most theories predict that α should be approximately proportional to r (*1*) and ν should be a universal constant based on hydrodynamic screening lengths [which Ogston *et al.* (*26*) and Alterberger and Tirrell (*28*) predict to be 1/2 (from quite different approaches), and others predict to be 2/3 or more (*29, 30*)]. The problem with Eq. 3 is that experimental measurements do not support any general correlation for α and ν, so that an a priori analytical treatment seems distant at present: α varies much more slowly than r; and ν, instead of being a universal constant, appears to vary between 0.38 and 2.21 even for very dilute polymer solutions (*31*). In our opinion, these problems stem from the difficulty in treating the microscopic equivalent of hydrodynamic "wall drag" and "tortuosity" through statistical mechanics. We present here a theoretical analysis that leads to a useful local viscosity relation for describing experimental data for diffusion processes. Predictions of this equation should be useful in analyzing sedimentation, polymerization, gel chromatography, and systems of biological and physiological interest.

We measured the viscosities and mutual diffusion coefficients of benzene–cyclohexane–dilute polymer solutions with techniques described elsewhere (*32, 33*). Polymer concentration and molecular weight strongly affect global viscosity (Fig. 1) so that for a polymer concentration of 2 g/dl and a molecular weight of 1.8 × 10^6, the viscosity of this three-component solution is almost 40 times that of cyclohexane-benzene without polymer. Although Eqs. 1 and 2 predict sharp decreases in diffusion coefficient with increased molecular weight or polymer concentration because of increases in viscosity, as does Eq. 3 for theoretical

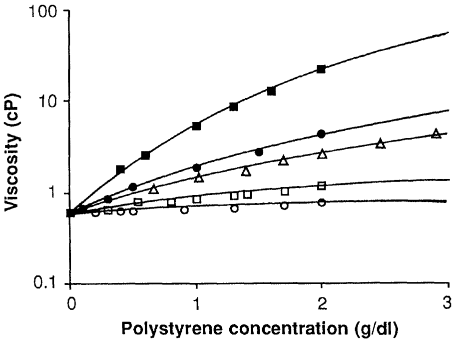

Fig. 1. Global viscosity of polystyrene-benzene-cyclohexane versus polystyrene concentration. Viscosities were measured with a Cannon-Ubbelohde viscometer; values for benzene and cyclohexane were compared with those in the literature (*41*), and the agreement was within 1%. Densities were measured with a pycnometer. Monodisperse polystyrene [MW_n = 4 × 10^3 (○), 5 × 10^4 (□), 6 × 10^5 (●), 1.8 × 10^6 (■); $MW_w/MW_n < 1.1$, where MW_n is the number-average molecular weight] was purchased from Alfa Products, and polydisperse polystyrene [MW_w = 3.21 × 10^5 (△), MW_w/MW_n = 3.8, where MW_w is the weight-average molecular weight] was purchased from Aldrich. All measurements were made at 25°C.

Department of Chemical Engineering, Michigan State University, East Lansing, MI 48824.

*To whom correspondence should be addressed.